

See discussions, stats, and author profiles for this publication at: <https://www.researchgate.net/publication/262534149>

# Switching Fluid Slippage on pH-Responsive Superhydrophobic Surfaces

ARTICLE *in* LANGMUIR · MAY 2014

Impact Factor: 4.46 · DOI: 10.1021/la500999k · Source: PubMed

---

CITATIONS

4

READS

65

## 6 AUTHORS, INCLUDING:



**Wu Yang**  
Chinese Academy of Sciences

12 PUBLICATIONS 42 CITATIONS

[SEE PROFILE](#)



**Xiaowei Pei**  
Chinese Academy of Sciences

25 PUBLICATIONS 340 CITATIONS

[SEE PROFILE](#)



**Feng Zhou**  
Chinese Academy of Sciences

257 PUBLICATIONS 6,304 CITATIONS

[SEE PROFILE](#)

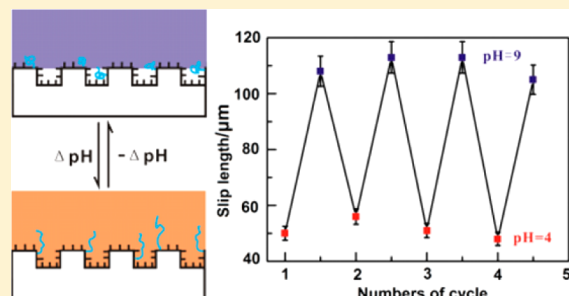
## Switching Fluid Slippage on pH-Responsive Superhydrophobic Surfaces

Yang Wu,<sup>†,‡</sup> Zhilu Liu,<sup>†</sup> Yongmin Liang,<sup>†</sup> Xiaowei Pei,<sup>\*,†</sup> Feng Zhou,<sup>\*,†</sup> and Qunji Xue<sup>†</sup>

<sup>†</sup>State Key Laboratory of Solid Lubrication, Lanzhou Institute of Chemical Physics, Chinese Academy of Sciences, Lanzhou 730000, P. R. China

<sup>‡</sup>University of Chinese Academy of Sciences, Beijing 100083, P. R. China

**ABSTRACT:** Two stimuli-responsive polymer brushes, poly(dimethylaminoethyl methacrylate) and poly(methacrylic acid), were grafted from initiator-modified anodized alumina substrates to prepare two pH-responsive surfaces. By regulating the swelling states of the two polymers, water droplets can roll off or adhere onto the textured surface because of different adhesion forces. These forces also strongly affect boundary slippage. To determine the different slippage effects of fluid on our pH-responsive surfaces, a series of rheological experiments are carried out on two kinds of surfaces. A large slip length is obtained and reversibly regulated by changing the fluid pH. These responsive superhydrophobic surfaces with considerable slip length and pH-responsive properties have extensive potential applications in intelligent micro- and nanofluidic devices or biodevices, which can solve fluid flow problems.



### INTRODUCTION

The wetting properties of water droplets have been a topic of interest for centuries.<sup>1,2</sup> Two typical wetting states, Cassie–Baxter state (superhydrophobic with low adhesion) and Wenzel state (superhydrophobic with high adhesion), are able to find their origins in nature.<sup>3,4</sup> But in recent years, researchers devoted to construct various superhydrophobic surfaces to biomimic but beyond what is in nature,<sup>5</sup> especially some environmental stimuli-responsive surfaces. By grafting some responsive polymer brushes onto rough substrates, scientists have access to regulate the surface wetting state from superhydrophobic to the superhydrophilic state<sup>6–9</sup> and to control the adhesion force<sup>10–12</sup> using the temperature, illumination, pH, electromagnetic field, and solvent. Superhydrophobic surfaces have become one of the top subjects in research because of their special wetting properties and potential applications, such as self-cleaning,<sup>13,14</sup> anti-icing,<sup>15,16</sup> anticorrosion,<sup>17</sup> antifouling,<sup>18</sup> and drag reducing.<sup>19,20</sup> Along with the appearance of micro- and nanofluidic devices, the drag reducing properties have drawn much attention because of the rapid increase of the surface-to-volume ratio. Rough hydrophobic surfaces or “superhydrophobic” surfaces have an “effective” liquid slip because the “liquid–solid shear” becomes “liquid–air shear” at the solid boundary.<sup>21</sup> In previous studies regarding the drag reduction of superhydrophobic surfaces, the microcosmic structures were emphasized. Truesdell<sup>22</sup> studied two surfaces with the same hydrophobic coating, one of which has regular grooves, while the other has a smooth surface. He found that longitudinal grooves are necessary to produce large slip length. Lee<sup>23</sup> achieved the maximum slip length of 400  $\mu\text{m}$  on dual-scale structures (micro–nano), which was larger than

the 100  $\mu\text{m}$  reported on single-scale (microsmooth) structures. His group has constructed different structures with “posts” and “grates” surfaces and varying gas fractions.<sup>24</sup> They found that for different samples with the target gas fraction fixed at the same value the slip length of the “grates” surfaces was larger than the “posts” surfaces. In addition, Ybert<sup>25</sup> obtained the scaling laws about the effective slip length at the surface, which possess generic surface characteristics such as roughness, length scale, depth, and solid fraction of the interface. Most of the above-mentioned studies focused on the surface morphology to influence the boundary slip. However, surface chemical modifications that affect the boundary slip are rarely reported, especially the cases where the surfaces are embedded with stimuli-responsive polymer brushes.

Many methods that detect the boundary slip have been reported. Examples of such methods are fluorescent recovery after photobleaching,<sup>26,27</sup> particle image velocimetry,<sup>28</sup> surface forces apparatus,<sup>29</sup> atomic force microscopy,<sup>30</sup> quartz crystal resonators,<sup>31</sup> capillary techniques,<sup>32</sup> and the rheometer method.<sup>33</sup> In rheological experiments, plate-and-plate arrangement is applied to record the shear stress at a constant shear rate, and a standard smooth stainless steel plate is used such that no-slip occurs when water flows on it. When two parallel plates are separated by a gap  $H$ , the slip length  $L_s$  of one of the two surfaces can be estimated using

Received: March 17, 2014

Revised: May 19, 2014

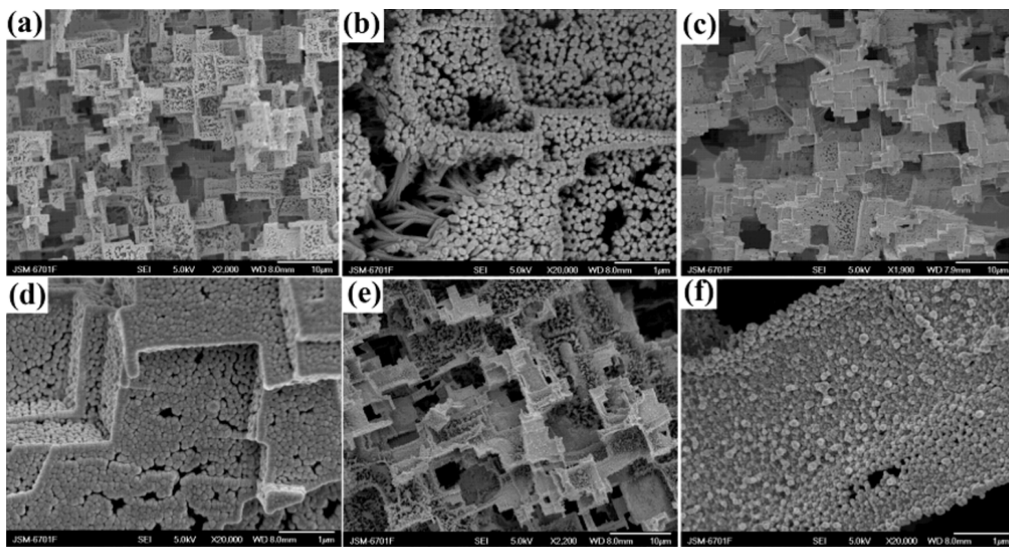


**Figure 1.** FE-SEM images of (a) anodized alumina; (c) pDMAEMA grafted anodized alumina (from initiator/PFOTS = 3:40); (e) pMAA grafted anodized alumina (from initiator/PFOTS = 5:40); (b), (d), and (f) are the respective magnified images.

$$\frac{\tau_{\text{slip}}}{\tau_{\text{no-slip}}} = \frac{1}{1 + \frac{L_s}{H}} \quad (1)$$

Moreover, the drag reduction efficiency  $D_R$  can be defined as

$$D_R = \frac{\tau_{\text{no-slip}} - \tau_{\text{slip}}}{\tau_{\text{no-slip}}} \quad (2)$$

where  $\tau_{\text{slip}}$  and  $\tau_{\text{no-slip}}$  are the shear stresses at the wall when slip and no-slip boundary conditions are applied, respectively. If the surface has boundary slip, the shear stress diminishes in contrast to without boundary slip.

In this work, we constructed two pH-responsive surfaces by grafting polymer brush on a rough anodized aluminum. The hydrophobic groups and responsive polymer brushes were introduced at the same time. The polymer brushes are able to swell or collapse because of their ability to acquire and lose protons under different pH conditions. Their different interactions with the water molecules can lead to different adhesion forces on the responsive surfaces by changing the pH of the droplets. To study the effect of the droplet adhesion force on the boundary slip, we carried out a series of rheological experiments to obtain the slip length of different pH conditions. In this method, a large slip length was obtained when the polymer molecules collapsed, whereas a relatively smaller slip length resulted when the polymer swelled. By regulating the pH of the fluid, the switchable slip length was observed on this responsive surface. These responsive surfaces can be applied to intelligent micro or smart fluidic devices to regulate flow.

## EXPERIMENTAL SECTION

**Materials and Chemicals.** Aluminum sheet (purity 99.99% Grinkin Advanced Materials Co., Ltd.), CuCl<sub>2</sub>·2H<sub>2</sub>O and oxalic acid (AR, Tianjin, China), 1H,1H,2H,2H-perfluorooctyltrichlorosilane (PFOTS, 97%, Aldrich), 2-(dimethylamino)ethyl methacrylate (DMAEMA, 99%, Aldrich), and methacrylic acid sodium (MAA, 99.5%, Aldrich) were used as received.

**Preparation of the Al<sub>2</sub>O<sub>3</sub> Substrate and Initiator Attachment.** The preparation of anodized alumina was carried out according to literature procedures.<sup>34</sup> The rough Al<sub>2</sub>O<sub>3</sub> sheets were cleaned by oxygen plasma for 3 min and were immersed in a solution of 50 mL of toluene containing a mixture of 3-(trichlorosilyl)propyl-2-bromo-2-

methylpropionate (initiator) and 1H,1H,2H,2H-perfluorooctyltrichlorosilane (PFOTS) in fixed molar ratios for 12 h. The samples were taken out of the mixed solution and copiously washed with hexane and ethanol and then blown dry with N<sub>2</sub>.

**Macromolecular Growth.** Surface-initiated atom transfer polymerization (SI-ATRP) of (dimethylamino)ethyl methacrylate (DMAEMA) according previous report.<sup>11</sup> 2.5 mL of DMAEMA monomer and 20 mL of 1:1 (v:v) MeOH–H<sub>2</sub>O mixture were placed in a reactor under a N<sub>2</sub> flow for 30 min; then, 0.0608 g of bipyridyl and 0.0304 g of CuBr were added into the reactor and blew with N<sub>2</sub> again; 20 min later the initiator–PFOTS decorated Al<sub>2</sub>O<sub>3</sub> sheets were added. The polymerization was performed at room temperature under N<sub>2</sub>. The substrate was taken out of the polymerization solution after 1 h and washed with plentiful ultrapure water and ethanol. Finally, the polymer grafted sheet was dried under vacuum overnight at 45 °C before further analysis. SI-ATRP of methylacrylic acid (MAA) was obtained by immersing the initiator–PFOTS modified sheets in a degassed solution of sodium methacrylate (1.5 g) in H<sub>2</sub>O and containing CuBr (0.015 g) and bipyridyl (0.030 g). The polymerization proceeded 4 h under N<sub>2</sub>, then washed with ultrapure water and ethanol and soaked in tetrahydrofuran to remove the physical absorption monomer, and finally dried under vacuum overnight at 60 °C before further analysis.

**Characterization.** Scanning electron microscope (SEM) images were obtained on a JSM-6701F field emission scanning electron microscope (FE-SEM) at 5–10 kV. X-ray photoelectron spectra (XPS) were obtained on a multifunctional XPS/AES system (Model PHI-5072, Physical Electronics, Inc., Eden Prairie, MN) by using Al K $\alpha$  radiation (250 W, pass energy of 29.35 eV). The binding energy of C<sub>1s</sub> (284.8 eV) was used as the reference. Sessile water droplet contact angle values were acquired using a DSA-100 optical contact angle meter (Kruss Company, Ltd., Germany) at ambient temperature (20 °C). 5  $\mu$ L of deionized water was dropped on the samples using an automatic dispense controller, and the contact angles were determined automatically by using the Laplace–Young fitting algorithm. The average contact angle values were obtained by measuring the sample at five different positions on the substrate. The adhesive force was measured by a high-sensitivity micro-electromechanical balance system (Dataphysics DCAT11, Germany). Water droplets suspended on a hydrophobic metal ring were approached and retracted from the sample surface at a constant speed. The droplet started to move away from the sample surface once in contact, and the balance force gradually increased and reached the maximum before the droplet broke away from the surface. The peak data recorded in the force–distance curve were taken as the break point adhesive force.

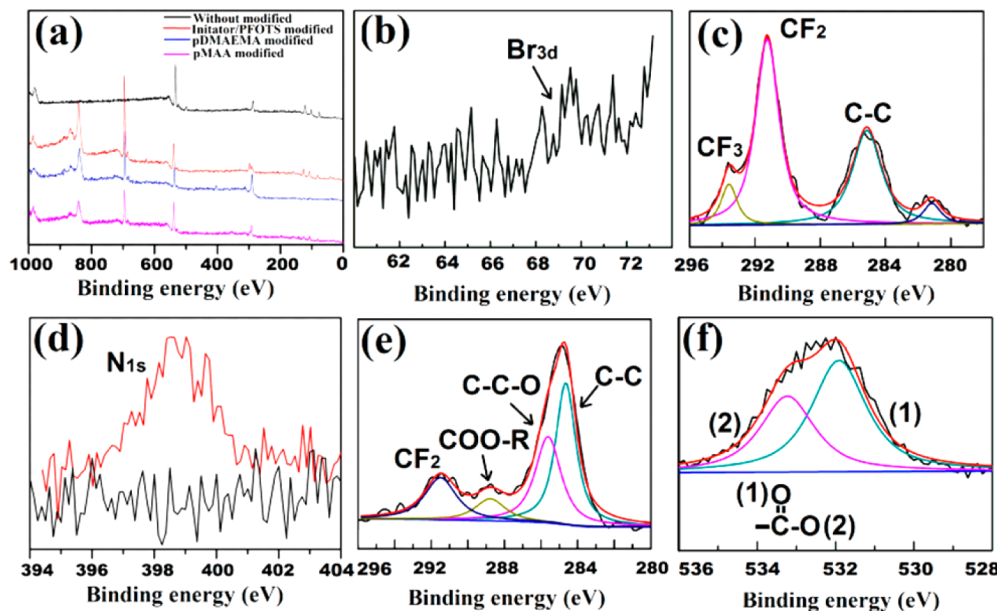


**Figure 2.** (a) XPS full spectra of the as-prepared sheets; fine spectra of (b) Br and (c) C element after modifying with initiator/PFOTS; (c) fine spectra of N element after grafting the pDMAEMA polymer brushes; and fine spectra of (e) C and (f) O element after grafting pMAA polymer brushes.

Boundary slippage was measured on a rheometer (HAAKE, RS6000, Germany). For this experiment, the plate-and-plate model was applied. A stainless steel clamp with a diameter ( $2R$ ) of 35 mm was used, and the modified anodized alumina was taken as a plate. The standard smooth stainless plate attached to the rheometer was considered the nonslip plate. Temperature was controlled with the error less 0.1 °C, and the distance ( $H$ ) between the clamp and test surface was measured by rheometer precisely. The fixed volume test liquid (buffered solution) was injected into the gap by a precise syringe. The clamp is driven by a given rotate speed with a certain angular velocity. If slip exists on a surface, the clamp will have different shear stress, which is recorded by the controlling computer. For the system with two parallel plates separated by a gap  $H$ , the slip length  $L_s$  of one of the two surfaces can be estimated by formula 1.

## RESULTS AND DISCUSSION

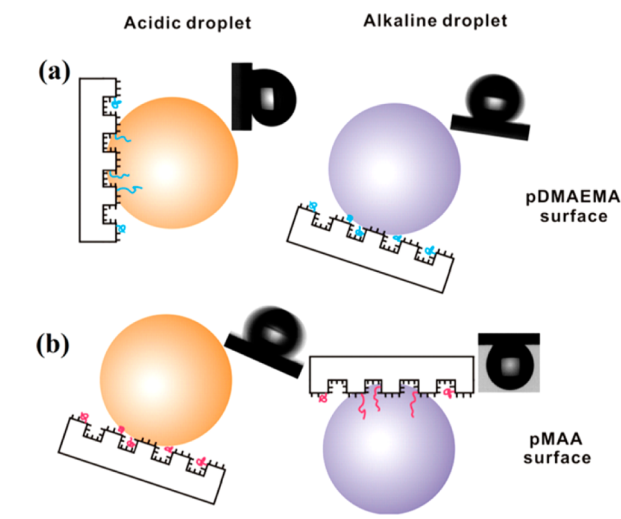
After the alternate anodized process, numerous irregular microscale step structures and nanowires structures (diameter ~100 nm) appeared on the alumina sheet, as shown in Figure 1a,b. The nanowires are neatly arranged and clearly show every wire, and the excellent oleophobic characteristics were endowed after being modified with a low-surface-energy material because of the dual structures.<sup>34,35</sup> Figures 1c,d and 1e,f are the FE-SEM images of the anodized alumina sheets grafted with pDMAEMA and pMAA brushes from initiator-PFOTS surface, respectively. It seems that the nanowires were grown on irregular microscale terrace structures. But compared with the SEM of anodized alumina without modification, the modified samples are covered by a layer of pDMAEMA polymer brushes, and some of the nanowire structures are even blocked. These results clearly proved that polymer brushes were successfully grafted on the anodized alumina. To prove our hypothesis, the chemical composition of these surfaces was analyzed using X-ray photoelectron spectra.

Figure 2a is the full XPS full spectra of all as-prepared sheets. After modifying the initiator-PFOTS and grafting the polymer brushes, the characteristic elements (F and N) appeared. Furthermore, the Al signal disappeared after grafting the polymer brush, which is due to that the photoelectrons cannot

penetrate the polymer coating. Figures 2b and 2c show the fine spectra of Br and C elements after modifying with the initiator-PFOTS, respectively. The single of Br sited at 69.8 eV is very weak because low concentration in stock solution and so on the surface. The four signal peaks of C element appeared because of the four different chemical bonds on the prepared anodized aluminum (Figure 2c). The peak at 281.2 eV was attributed to the chemically shift of C 1s. After grafting the pDMAEMA polymer chains, the N 1s signal at 399.2 eV indicated the presence of the pDMAEMA polymer brush as seen from Figure 2d. Figures 2e and 2f show a high-resolution scan of the C 1s and O XPS survey spectra of the sheet after modifying with pMAA brush. In agreement with the elemental composition of pMAA, the carbon atom of the carboxyl group can be clearly distinguished and was shifted about 4 to 288.5 eV. The oxygen element spectra of pMAA brush sited at 531.8 and 533.2 eV were distinguishable and ascribed to two different oxygen atoms of carboxyl. Through the above discussion, we concluded that the two kinds of polymer brushes were grafted on the rough surface successfully.

The adhesion force is another important property of the surface aside from the wetting state. Here, we introduced the hydrophobic group PFOTS aimed at keeping the wetting state unchanged, but varying the adhesion force by grafting polymer brushes. DMAEMA is a kind of weak base and has a  $pK_a$  of 7. After grafting the weak base monomers on the solid surface, the polymer brushes will show hydrophobic collapse in basic environments and hydrophilic swelling in acid environments caused by the deprotonation and protonation of the amine groups, respectively. Therefore, the rough surface modified with pDMAEMA polymer brush has a pH-responsive character. For droplets with different pH, the surface adhesion was also different on the polymer surface. Scheme 1a shows that because of the low surface adhesion of a basic droplet (pH 9), the droplet rolls down with slight tilt. However, for an acidic droplet (pH 4), a high adhesion was observed. To the contrary, MAA is a weak acid with  $pK_a$  of 4.8. The pMAA polymer brushes show a hydrophobic collapsed state in acidic

**Scheme 1.** Schematic of Interchangeable Adhesion of the Surface Grafted with (a) pDMAEMA and (b) pMAA with Acidic and Alkaline Droplet, Respectively



environments and a hydrophilic swollen state in basic environments because of the protonation and deprotonation of the carboxyl groups, respectively. Therefore, for droplets with different pH, different adhesion forces will result, as shown in Scheme 1b. Low adhesion for an acidic droplet (pH 4) was observed, and the droplet can roll down with a slight tilt. However, for an alkaline droplet (pH 9) high adhesion was observed and was adhered on the surface even though the surface was overturned.

The quantified adhesion force values of several droplets ranging from pH 4 to 9 on the pDMAEMA and pMAA grafted substrate are shown in Figure 3. Figure 3a shows the adhesion force curves of droplets on the pDMAEMA surface, and the values are summarized in Figure 3b. From the two figures, we find that the adhesion force between the acidic droplet (pH 4) and the pDMAEMA surface is  $81 \pm 5.0 \mu\text{N}$ . For the acidic droplets, an increase in the pH caused the adhesion force to slightly decrease from 81 to  $68 \pm 4.0 \mu\text{N}$ . The main reason here is the

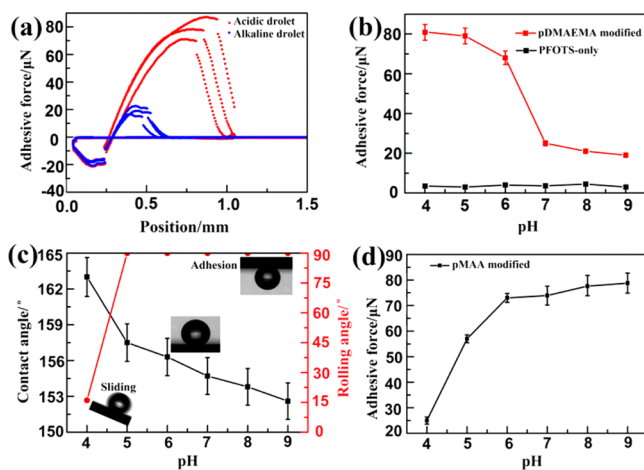


**Figure 3.** (a) Adhesion force curves of various pH droplets on the pDMAEMA grafted substrate and (b) corresponding adhesion force values on pDMAEMA grafted and PFOTS-only substrate. (c) Contact and sliding angles and (d) adhesion force on a pMAA modified substrate (initiator/PFOTS = 5/40).

proton concentration and the reduced level of protonated amine groups. When the pH increased to 7, the adhesion sharply decreased from  $68 \pm 4.0$  to  $25 \pm 2.2 \mu\text{N}$ . When the pH of droplet was 9, the adhesion had a minimum value of about  $19 \pm 1.0 \mu\text{N}$ . To reveal the role of pDMAEMA brush, the adhesion force between the pH droplets and the PFOTS-only modified surface also was detected. When the droplets were close to the PFOTS-only modified surface, the surface adhesion was kept at a very small value of about  $5 \mu\text{N}$  and independent of the pH of those droplet (Figure 3b). However, the adverse results of pMAA surface were obtained and shown in Figure 3c,d. Figure 3c shows the static contact and sliding angles of several droplets with pH ranging from 4 to 9 on the pMAA grafted substrate (from initiator-PFOTS 5:40). The surface was kept at a superhydrophobic state ( $>150^\circ$ ) for these droplets, and the contact angle decreased as the pH of the droplets increased. Only under a low pH value (pH 4) can the droplet can slide off the surface freely. When pH increased (5–9), the droplets adhered onto the surface even as the surface was overturned. The corresponding adhesion force between the acidic droplet (pH 4) and the substrate was only just  $25 \pm 1.5 \mu\text{N}$ , as shown in Figure 3d. In addition, when the pH increased to 5 and 6, the adhesion increased to  $57 \pm 3.0$  and  $73 \pm 4.0 \mu\text{N}$ , respectively. The main reason was the concentration of proton and the increased level of deprotonation of the carboxyl groups. When the pH increased (7–9), the adhesion was also increased to high value and remained about  $80 \pm 4.0 \mu\text{N}$ .

Surface adhesion affects the boundary slippage,<sup>36</sup> and the slip length decays with the increasing adhesion force. Here, we discuss the Couette flow slippage on these pH-responsive surfaces. Using the rheometer method, the shear stress of the fluid that flowed over the as-prepared pH-responsive superhydrophobic surfaces was measured, and the slip length was calculated using formula 1 and summarized in Figure 4. For PFOTS-only modified surface, the slip length kept a fixed value of about  $130 \mu\text{m}$ . The slip length has no relation with the pH of the fluid, but for the pDMAEMA modified surface, a different situation emerged. For acidic solution (pH 4–6), the fluid slip length was about  $50$ – $60 \mu\text{m}$  (Figure 4a). But for alkaline solution, the slip length can reach  $110 \mu\text{m}$ . For previous report, an interchangeable boundary slip is rarely reported. However, our pH-responsive surface embedded with pDMAEMA polymer brushes has a interchangeable regulation characteristic. After every slip test, a simple treatment with distilled water and ethanol was taken for the responsive surface, and the surface again possesses the same adhesive characteristic as before. The several switching cycles were achieved from about  $50$  to  $110 \mu\text{m}$  by changing the pH of the solution from 4 to 9, as shown in Figure 4b. Similar with the pDMAEMA modified surface, the slip measurement of the pMAA modified surface also was studied, and the opposite results were obtained. As shown in Figure 4c, the maximum value of slip length was about  $110 \mu\text{m}$  for the acidic solution (pH 4). When the pH increased to 5, the slip length drastically decreased to  $57 \mu\text{m}$ . When the pH increased from 5 to 9, the slip length slightly decreased from  $57$  to  $40 \mu\text{m}$ . The interchangeable cycles also can be achieved similar to the pDMAEMA modified surface (Figure 4d).

As we know, the Wenzel state (superhydrophobic with high adhesion) is metastable state, and the wetting state is changed easily when suffering external stress. Conversely, the Cassie–Baxter state (superhydrophobic with low adhesion) is a stable state, and the wetting state cannot be changed easily under external stress. Our pH-sensitive surfaces can possess the two

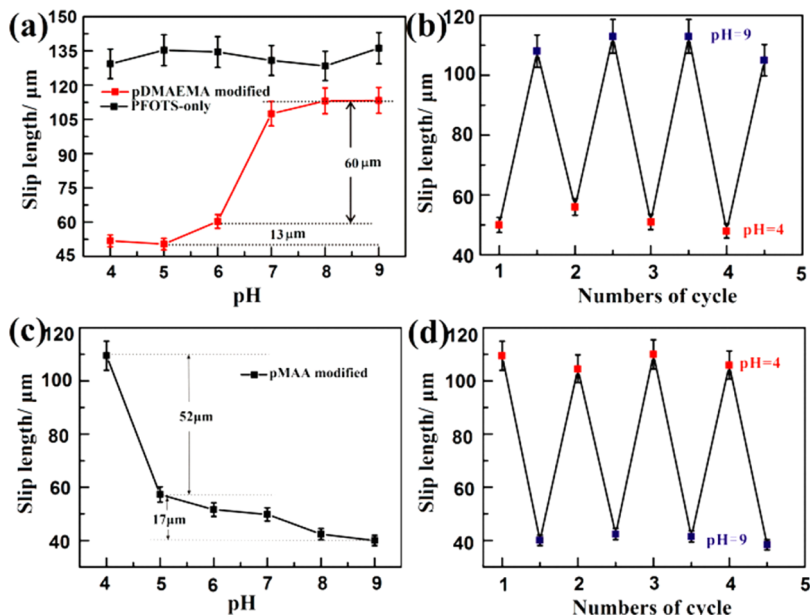


**Figure 4.** Slip length of (a) pDMAEMA polymer brush, PFOTS-only modified and (c) pMAA brush modified surface. (b) Reversible switching the slip length on (c) pDMAEMA and (d) pMAA surface by changing pH of fluid.

states by changing the pH of droplet. Taking the surface modified with pDMAEMA brush as an example, an acidic droplet adhered on the surface with Wenzel state, but an alkaline droplet slide with Cassie–Baxter state (Scheme 1a). Because of the narrow gap and sheer stress of rheometer, the acidic solution wet up the pDMAEMA modified surface after the slip measurement, as shown in Figure 5a. Though the

acidic and alkaline solution ( $\sim 60 \mu\text{m}$ ) can be assumed to be caused by the different wetting state changes for different pH conditions during the slip measurement. When liquid wetted surface, the air bubbles between the liquid and solid interface are discharged such that the air fraction between the two interfaces decreases to reduce the boundary slip, as shown in Figure 5c,d. To study the influence of the lubricating gas film between the solid and liquid surface, Lee<sup>40</sup> constructed a self-controlled gas-generating superhydrophobic surface, and the same conclusion was reached. The boundary slip vanished when the surface wetted, and the slippage emerged again when the microbubbles were produced.

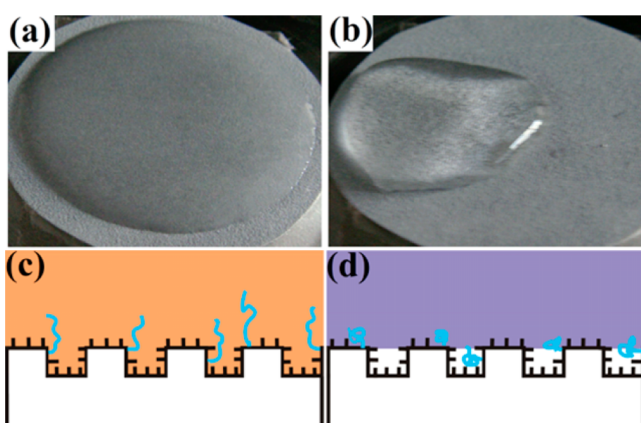


**Figure 5.** Images of (a) acidic and (b) alkaline test solutions on a pDMAEMA brush sheet after the slip measurement and the corresponding schematic under (c) acidic and (d) alkaline environment.

surface was wetted, a slip length ( $\sim 50 \mu\text{m}$ ) was still obtained mainly because the modified surface had a larger contact angle than the reference stainless steel plate.<sup>37–39</sup> Under the narrow gap of the rheometer, a higher contact angle led to a smaller contact area as well as to a smaller torque. Influenced by these, the calculated value using formula 1 was higher. But for alkaline solution, the wetting state did not change and was still kept in a Cassie state after the slip measurement, as shown in Figure 5b. The larger slip length ( $\sim 110 \mu\text{m}$ ) can be attributed to the edge effect and nonwetted appearance similar to the PFOTS-only modified sheet. The different slip length values between the

## CONCLUSIONS

pH-sensitive pDMAEMA and pMAA polymer brushes were grafted onto a rough anodized aluminum using SI-ATRP to prepare two pH-responsive surfaces. The two pH-sensitive surfaces were able to keep a superhydrophobic state for a series of pH solution and showed different adhesive properties due to the different  $pK_a$  of two monomers. The rheological experiments of the pH solution flowing over responsive surfaces have proved the existence of the slippage effect at the responsive interface between the liquid and the modified surface. The slip length and adhesion force can be regulated by changing the pH of solution. The surface wetting state was not easily transformed, and a large slip length was obtained when the polymer shrank. As the polymer swelled, the surface wetting state transformed easily, and a smaller slip length was obtained. When a fluid flows on our coated surface it would lead to a 10% drag reduction. If the devices are downsized, the boundary affect between the liquid and solid interface is clearer,<sup>41</sup> and the difference of slip length are increased for acidic and basic solutions. The surfaces capable of a considerable slippage effect have broad potential for application in intelligent microfluidic devices and biodevices to help regulate quantity of flow in situ.

## AUTHOR INFORMATION

### Corresponding Authors

\*E-mail zhouf@licp.cas.cn (F.Z.).  
\*E-mail peixw@licp.cas.cn (X.P.).

### Notes

The authors declare no competing financial interest.

## ACKNOWLEDGMENTS

This work was financially supported by NSFC (21125316, 51305428, 51335010) and Key Research Program of CAS (KJZD-EW-M01).

## REFERENCES

- (1) Wenzel, R. N. Resistance of Solid Surfaces to Wetting by Water. *Ind. Eng. Chem.* **1936**, *28*, 988–994.
- (2) Cassie, A. B. D.; Baxter, S. Wettability of Porous Surfaces. *Trans. Faraday Soc.* **1944**, *40*, 546–551.
- (3) Feng, L.; Zhang, Y.; Xi, J.; Zhu, Y.; Wang, N.; Xia, F.; Jiang, L. Petal Effect: A Superhydrophobic State with High Adhesive Force. *Langmuir* **2008**, *24*, 4114–4119.
- (4) Neinhuis, C.; Barthlott, W. Characterization and Distribution of Water-Repellent, Self-Cleaning Plant Surfaces. *Ann. Bot.* **1997**, *79*, 667–677.
- (5) Liu, X.; Liang, Y.; Zhou, F.; Liu, W. Extreme Wettability and Tunable Adhesion: Biomimicking Beyond Nature? *Soft Matter* **2012**, *8*, 2070–2086.
- (6) Xu, L.; Chen, W.; Mulchandani, A.; Yan, Y. Reversible Conversion of Conducting Polymer Films from Superhydrophobic to Superhydrophilic. *Angew. Chem., Int. Ed.* **2005**, *44*, 6009–6012.
- (7) Sun, T.; Wang, G.; Feng, L.; Liu, B.; Ma, Y.; Jiang, L.; Zhu, D. Reversible Switching between Superhydrophilicity and Superhydrophobicity. *Angew. Chem., Int. Ed.* **2004**, *43*, 357–360.
- (8) Lim, H. S.; Han, J. T.; Kwak, D.; Jin, M. H.; Cho, K. Photoreversibly Switchable Superhydrophobic Surface with Erasable and Rewritable Pattern. *J. Am. Chem. Soc.* **2006**, *128*, 14458–14459.
- (9) Minko, S.; Müller, M.; Motornov, M.; Nitschke, M.; Grundke, K.; Stamm, M. Two-level Structured Self-Adaptive Surfaces with Reversibly Tunable Properties. *J. Am. Chem. Soc.* **2003**, *125*, 3896–3900.
- (10) Liu, X.; Cai, M.; Liang, Y.; Zhou, F.; Liu, W. Photo-regulated Stick-Slip Switch of Water Droplet Mobility. *Soft Matter* **2011**, *7*, 3331–3336.
- (11) Liu, X.; Ye, Q.; Yu, B.; Liang, Y.; Liu, W.; Zhou, F. Switching Water Droplet Adhesion Using Responsive Polymer Brushes. *Langmuir* **2010**, *26*, 12377–12382.
- (12) Cheng, Z.; Feng, L.; Jiang, L. Tunable Adhesive Superhydrophobic Surfaces for Superparamagnetic Microdroplets. *Adv. Funct. Mater.* **2008**, *18*, 3219–3225.
- (13) Fürstner, R.; Barthlott, W. Wetting and Self-Cleaning Properties of Artificial Superhydrophobic Surfaces. *Langmuir* **2005**, *21*, 956–961.
- (14) Nakajima, A.; Hashimoto, K.; Watanabe, T. Transparent Superhydrophobic Thin Films with Self-Cleaning Properties. *Langmuir* **2000**, *16*, 7044–7047.
- (15) Cao, L.; Jones, A. K.; Sikka, V. K.; Wu, J.; Gao, D. Anti-Icing Superhydrophobic Coatings. *Langmuir* **2009**, *25*, 12444–12448.
- (16) Mishchenko, L.; Hatton, B.; Bahadur, V.; Taylor, J. A.; Krupenkin, T.; Aizenberg, J. Design of Ice-free Nanostructured Surfaces Based on Repulsion of Impacting Water Droplets. *ACS Nano* **2010**, *4*, 7699–7707.
- (17) Xu, Q. F.; Wang, J. N. A Superhydrophobic Coating on Aluminium Foil with An Anti-corrosive Property. *New J. Chem.* **2009**, *33*, 734–738.
- (18) Pan, S.; Kota, A. K.; Mabry, J. M.; Tuteja, A. Superomniphobic Surfaces for Effective Chemical Shielding. *J. Am. Chem. Soc.* **2013**, *135*, 578–581.
- (19) McHale, G.; Newton, M. I.; Shirtcliffe, N. J. Immersed Superhydrophobic Surfaces: Gas Exchange, Slip and Drag Reduction Properties. *Soft Matter* **2010**, *6*, 714–719.
- (20) Wu, Y.; Cai, M.; Li, Z.; Song, X.; Wang, H.; Pei, X.; Zhou, F. Slip Flow of Diverse Liquids on Robust Superomniphobic Surfaces. *J. Colloid Interface Sci.* **2014**, *414*, 9–13.
- (21) Vinogradova, O. I. Drainage of a Thin Liquid Film Confined between Hydrophobic Surfaces. *Langmuir* **1995**, *11*, 2213–2220.
- (22) Truesdell, R.; Mammoli, A.; Vorobieff, P.; Swol, F.; Brinker, C. Drag Reduction on a Patterned Superhydrophobic Surface. *Phys. Rev. Lett.* **2006**, *97*, 044504.
- (23) Lee, C.; Kim, C.-J. Maximizing the Giant Liquid Slip on Superhydrophobic Microstructures by Nanostructuring Their Side-walls. *Langmuir* **2009**, *25*, 12812–12818.
- (24) Lee, C.; Choi, C.-H.; Kim, C.-J. Structured Surfaces for a Giant Liquid Slip. *Phys. Rev. Lett.* **2008**, *101*, 064501.
- (25) Ybert, C.; Barentin, C.; Cottin-Bizonne, C.; Joseph, P.; Bocquet, L. Achieving Large Slip with Superhydrophobic Surfaces: Scaling Laws for Generic Geometries. *Phys. Fluids* **2007**, *19*, 123601.
- (26) Pit, R.; Hervet, H.; Léger, L. Friction and Slip of A Simple Liquid at A Solid Surface. *Tribol. Lett.* **1999**, *7*, 147–152.
- (27) Hervet, H.; Léger, L. Flow with Slip at The Wall: from Simple to Complex Fluid. *C. R. Phys.* **2003**, *4*, 241–249.
- (28) Joseph, P.; Tabeling, P. Direct Measurement of the Apparent Slip Length. *Phys. Rev. E* **2005**, *71*, 035303.
- (29) Zhu, Y.; Granick, S. Rate-Dependent Slip of Newtonian Liquid at Smooth Surfaces. *Phys. Rev. Lett.* **2001**, *87*, 096105.
- (30) Henry, C. L.; Neto, C.; Evans, D. R.; Biggs, S.; Craig, V. S. J. The Effect of Surfactant Adsorption on Liquid Boundary Slippage. *Physica A* **2004**, *339*, 60–65.
- (31) Du, B.; Goubaudouline, I.; Johannsmann, D. Effects of Laterally Heterogeneous Slip on the Resonance Properties of Quartz Crystals Immersed in Liquids. *Langmuir* **2004**, *20*, 10617–10624.
- (32) Choi, C. H.; Ulmanella, U.; Kim, J.; Ho, C.-M.; Kim, C. J. Effective Slip and Friction Reduction in Nanograted Superhydrophobic Microchannels. *Phys. Fluids* **2006**, *18*, 087105.
- (33) Choi, C. H.; Kim, C. J. Large Slip of Aqueous Liquid Flow over a Nanoengineered Superhydrophobic Surface. *Phys. Rev. Lett.* **2006**, *96*, 066001.
- (34) Wu, W.; Wang, X.; Wang, D.; Chen, M.; Zhou, F.; Liu, W.; Xue, Q. Alumina Nanowire Forests via Unconventional Anodization and Super-repellency plus Low Adhesion to Diverse Liquids. *Chem. Commun.* **2009**, 1043–1045.
- (35) Liu, X.; Wang, X.; Liang, Y.; Bell, S. E. J.; Liu, W.; Zhou, F. Superoleophobicity under Vacuum. *Appl. Phys. Lett.* **2011**, *98*, 194102.
- (36) Wu, Y.; Xue, Y.; Pei, X.; Cai, M.; Duan, H.; Huck, W. T. S.; Zhou, F.; Xue, Q. Adhesion-Regulated Switchable Fluid Slippage on Super-hydrophobic Surfaces. *J. Phys. Chem. C* **2014**, *118*, 2564–2569.
- (37) Li, J.; Zhou, M.; Ye, X.; Cai, L. Self-comparison Measurement for Slippage on Superhydrophobic Surfaces Based on the Wetting Transition. *J. Micromech. Microeng.* **2010**, *20*, 115022.
- (38) Bocquet, L.; Tabeling, P.; Manneville, S. Comment on ‘Large Slip of Aqueous Liquid Flow over a Nanoengineered Superhydrophobic Surface’. *Phys. Rev. Lett.* **2006**, *97*, 109601.
- (39) Zhou, M.; Li, J.; Wu, C. X.; Zhou, X. K.; Cai, L. Fluid Drag Reduction on Superhydrophobic Surfaces Coated with Carbon Nanotube Forests (CNTs). *Soft Matter* **2011**, *7*, 4391–4396.
- (40) Lee, C.; Kim, C. J. Underwater Restoration and Retention of Gases on Superhydrophobic Surfaces for Drag Reduction. *Phys. Rev. Lett.* **2011**, *106*, 014502.
- (41) Squires, T. M. Microfluidics: Fluid Physics at the Nanoliter Scale. *Rev. Mod. Phys.* **2005**, *77*, 977–1026.